Plasmonics (2017) 12:1717–1723
DOI 10.1007/s11468-016-0438-4

Inverse Design of Dielectric Resonator Cloaking Based on Topology Optimization

Yongbo Deng[1] · Zhenyu Liu[2] · Yongmin Liu[3,4] · Yihui Wu[1]

Received: 12 August 2016 / Accepted: 9 November 2016 / Published online: 22 November 2016

Abstract In many applications, a cloaked resonator is highly desired, which can harvest and maximize the energy within the resonator without being detected. This paper presents the resonator cloaking achieved by topology optimization-based inverse design methodology. The resonator cloaking is inversely designed by solving the topology optimization problem with minimizing the ratio of the scattering field energy outside the cloak and the cloaked resonating field energy. By inversely designing the resonator cloaking with relative permittivity 2 for both the resonator and cloak, the topology optimization-based inverse design methodology is demonstrated, where the incident angle sensitivity is considered to derive incident angle insensitive design. Then, the proposed methodology is applied for the cases with resonator and cloak materials chosen from dielectrics with low, moderate and high permittivity, respectively. The derived results demonstrate that the resonator cloaking can be categorized into three types, which are the Fabry-Pérot resonance cloaking, Mie resonance cloaking and hybrid resonance cloaking.

Keywords Resonator cloaking · Inverse design · Topology optimization · Fabry-pérot resonance cloaking · Mie resonance cloaking · Hybrid resonance cloaking

✉ Yongbo Deng
dengyb@ciomp.ac.cn

[1] State Key Laboratory of Applied Optics, Changchun Institute of Optics, Fine Mechanics and Physics (CIOMP), Chinese Academy of Sciences, Changchun, 130033, China

[2] Changchun Institute of Optics, Fine Mechanics and Physics (CIOMP), Chinese Academy of Sciences, Changchun, 130033, China

[3] Department of Mechanical and Industrial Engineering, Northeastern University, Boston, MA, 02115, USA

[4] Department of Electrical and Computer Engineering, Northeastern University, Boston, MA, 02115, USA

Introduction

Many different applications are in pressing need of effectively cloaking resonators (or sensors and detectors), which can efficiently detect signals but has negligible disturbance on the surrounding environment. For example, in physics and engineering experiments, this means that a probe, e.g. the tip of a near-field scanning optical microscope or a microwave antenna, may have a minimal scattering effect on the quantity it is designed to measure [1, 2]. With the development of transformation optics, the old dream of a device which render an object invisible to the human eye is already within reach [3, 4]. By transformation optics, the cloak/anticloak interaction has been investigated to realize the sensor cloaking [5]. However, the derived cloak/anticloak has extreme electromagnetic properties, permittivity and permeability. And they normally are implemented by exotic metamaterials [6]. The tailored microstructure of such metamaterials has to be much smaller than the wavelength, and this makes it very challenging to realize the desired magnetic properties at optical frequencies. Would it be possible to design a cloaked resonator using conventional simple isotropic dielectric readily

available in nature instead of using metamaterials with extreme electromagnetic properties?

To address this question, we adopt an inverse design approach based on topology optimization to find the geometrical configuration of the conventional nonmagnetic isotropic dielectric cloak for a resonator. Besides, the metasurfaces-based electromagnetic illusion or virtual shaping has also been demonstrated to be an alternative approach [7–9]. Topology optimization is a full-parameter method used to inversely determine the geometrical configuration, which represents distribution of materials [10]. It can be used to implement the structural design for the cases where the scale is large enough to ensure the reasonability for using physical parameters of materials fitting in with statistical hypothesis or continuum hypothesis. In contrast to designing devices by tuning a handful of structural parameters in size and shape optimization, topology optimization method utilizes the full-parameter space to design structures solely based on the user's desired performance specification. Therefore, topology optimization is more flexible and robust, because of its low dependence on initial structure and implicitly expression of the material distribution in structures. Further, topology optimization can inversely determine the geometrical configuration representing simultaneously the structural topology, shape and size; and it is a more general computational design methodology. Topology optimization has been applied to multiple physical problems, such as elastics, acoustics, electromagnetics, fluidics, optics, thermal dynamics, and material design problems [10]. In electromagnetics, it has been applied in the inverse design of cloaks, splitter, photonic crystal, plasmonic nanostructures, dielectric metamaterials [18–22], to name the most prominent. Therefore, topology optimization is one reasonable approach to achieve resonator cloaking.

Methodology

An infinitely long cylinder domain is illuminated in the free space with monochromatic propagating wave. Due to the invariance of the electromagnetic properties along the cylinder axis, the problem can be formulated in a plane perpendicular to the cylinder axis. A firs- order absorbing boundary condition is used as an approximation to the Sommerfeld radiation condition in order to truncate the infinite domain. Thus, the computational domain is preset as shown Fig. 1 with one circularly-shaped resonator at the center. A time-harmonic electromagnetic wave propagates from the left boundary through the computational domain. In the computational domain, the resonator cloak is located in a ring-shaped domain with the same center as the resonator, and it is inversely determined using the topology optimization approach. The rest surrounding medium is set

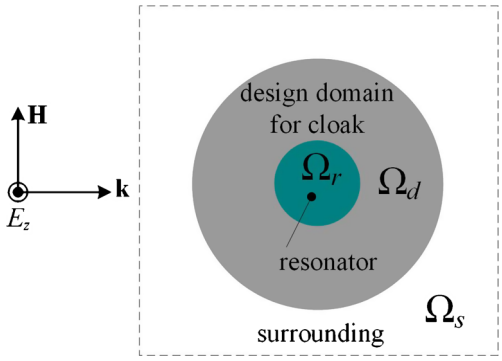

Fig. 1 Sketch for the computational domain. The resonator Ω_r is located at the center of the computational domain; the ring-shaped design domain Ω_d for the cloak surrounds the resonator; and the outside surrounding Ω_s is set to be vacuum

to be vacuum. For transverse electric (TE) polarization, the waves are described by the governing equation as follows

$$\begin{aligned} \nabla \cdot \left[\mu_r^{-1} \nabla \left(E_{zs} + E_{zi}\right)\right] + k_0^2 \epsilon_r \left(E_{zs} + E_{zi}\right) &= 0, \text{ in } \Omega \\ \mu_r^{-1} \nabla E_{zs} \cdot \mathbf{n} + j k_0 \sqrt{\epsilon_r \mu_r^{-1}} E_{zs} &= 0, \text{ on } \partial\Omega \end{aligned} \tag{1}$$

where E_{zs} is the scattering TE field; E_{zi} is the incident TE field; ϵ_r and μ_r are the relative permittivity and permeability, respectively; k_0 is the free space wave number; j is the imaginary unit; Ω is the computational domain with trace $\partial\Omega$. This paper considers the inverse design case for uniform plane incident waves with the incident TE wave E_{zi} set to be $e^{-jk_0\mathbf{k}\cdot\mathbf{x}}$, where $\mathbf{k}$ is the normalized wave vector and $\mathbf{x}$ is the spatial coordinate.

Topology optimization approach is based on the material interpolation between two different materials. And the material interpolation is implemented with the binary distribution defined in the design domain, where the binary distribution with values 0 and 1 respectively represent two material phases. This paper considers nonmagnetic materials with unity relative permeability. Then, the inverse design for the resonator cloaking is focused on the geometrical configuration corresponding to the spatial distribution of materials with two different relative permittivity. The binary distribution is set to be the design variable, which is relaxed to vary in the interval $[0, 1]$ in the gradient information-based topology optimization. To regularize the relaxed design variable continuously valued in $[0, 1]$ and converge to one binary distribution at the end of the topology optimization procedure, the design variable is filtered using the Helmtoltz equation-based PDE filter [23]

$$\begin{aligned} -\nabla \cdot \left(r^2 \nabla \gamma_f\right) + \gamma_f &= \gamma, \text{ in } \Omega_d \\ \nabla \gamma_f \cdot \mathbf{n} &= 0, \text{ on } \partial\Omega_d \end{aligned} \tag{2}$$

where γ is the design variable defined on the design domain, and Ω_d is the design domain set to be the ring-shaped cloak domain that surrounds the resonator. The filtered design variable is projected by the threshold method [24]

$$\gamma_p = \frac{\tanh(\beta\xi) - \tanh\left(\beta\left(\gamma_f - \xi\right)\right)}{\tanh(\beta\xi) - \tanh(\beta(1-\xi))} \tag{3}$$

where r is the filter radius chosen based on numerical experiments [23]; γ_f is the filtered design variable; γ_p is the projected design variable named physical density representing the geometrical configuration [25]; $\xi \in [0, 1]$ and β are the threshold and projection parameters for the threshold projection, respectively: ξ is set to be 0.5, and β is set with initial value 1 and it is doubled every 40 iterations [26]. Then, the material interpolation is implemented using the projected design variable as

$$\epsilon_r = \epsilon_{rl} + \gamma_p\left(\epsilon_{ru} - \epsilon_{rl}\right) \tag{4}$$

where ϵ_{rl} and ϵ_{ru} are the relative permittivity of two different dielectrics, respectively.

In this inverse design method, the resonator cloak is determined based on its desired resonator cloaking performance, that is the total electric field should be enhanced in the resonating domain and the scattering field should be weakened or nearly removed in the outside surrounding of the resonator cloak. The scattering field induced in the surrounding of resonator cloak can be measured by

$$\Psi_{Es} = \frac{1}{\Psi_{Es0}}\int_{\Omega_s} E_{zs}E_{zs}^*\,\mathrm{d}\Omega \tag{5}$$

where the asterisk denotes the complex conjugate, Ψ_{Es0} is the reference value equal to the norm of the scattering TE field, induced by the uncloaked resonator, in the outside cloak surrounding Ω_s. The total field in the resonator can be measured by

$$\Psi_{Er} = \frac{1}{\Psi_{Er0}}\int_{\Omega_r}\left(E_{zs}+E_{zi}\right)\left(E_{zs}+E_{zi}\right)^*\,\mathrm{d}\Omega \tag{6}$$

where Ψ_{Er0} is the reference value equal to the norm of the total TE field inside the uncloaked resonator in Ω_r. Then, the inversely determined resonator cloaking should correspond to the minima of the quotient between the norms of the scattering field in the surrounding of resonator cloak and total field in the resonator

$$q = \frac{\Psi_{Es}}{\Psi_{Er}} \tag{7}$$

As a result, one variational problem for inverse design of resonator cloaking can be built by minimizing the quotient in Eq. 7 constrained by the TE wave equation in Eq. 1. To solve this variational problem, the gradient-based optimization algorithm is used to derive the geometrical configuration for the resonator cloaking, where the design variable is iteratively evolved with the gradient information derived by the adjoint analysis. The gradient information is used to determine the evolution direction of the design variable. The adjoint analysis-derived gradient for the quotient in Eq. 7 is

$$\delta q = \frac{\delta\Psi_{Es}}{\Psi_{Er}} - \frac{\Psi_{Es}}{\Psi_{Er}^2}\delta\Psi_{Er} \tag{8}$$

In Eq. 8, $\delta\Psi_{Es}$ is the first-order variational of Ψ_{Es}

$$\delta\Psi_{Es} = -\int_{\Omega_d}\tilde{\gamma}_f\delta\gamma\,\mathrm{d}\Omega \tag{9}$$

with $\tilde{\gamma}_f$ derived by solving the adjoint equations

$$\begin{aligned}
&\int_\Omega \frac{2E_{zs}^*}{\Psi_{Es0}}\tilde{\tilde{E}}_{zs} - \mu_r^{-1}\nabla\tilde{E}_{zs}^*\cdot\nabla\tilde{\tilde{E}}_{zs} + k_0\epsilon_r\tilde{E}_{zs}^*\tilde{\tilde{E}}_{zs}\,\mathrm{d}\Omega\\
&-\int_{\partial\Omega} jk_0\sqrt{\epsilon_r\mu_r^{-1}}\tilde{E}_{zs}^*\tilde{\tilde{E}}_{zs}\,\mathrm{d}\Gamma = 0,\\
&\int_{\Omega_d} r^2\nabla\tilde{\gamma}_f\cdot\nabla\tilde{\tilde{\gamma}}_f + \tilde{\gamma}_f\tilde{\tilde{\gamma}}_f + k_0\frac{\partial\epsilon_r}{\partial\gamma_p}\frac{\partial\gamma_p}{\partial\gamma_f}\Big[Re\left(E_{zs}+E_{zi}\right)\\
&Re\left(\tilde{E}_{zs}^*\right) - Im\left(E_{zs}+E_{zi}\right)Im\left(\tilde{E}_{zs}^*\right)\Big]\tilde{\tilde{\gamma}}_f\,\mathrm{d}\Omega = 0,\\
&\forall\tilde{\tilde{E}}_{zs}\in\mathcal{H}(\Omega),\ \forall\tilde{\tilde{\gamma}}_f\in\mathcal{H}(\Omega_d)
\end{aligned} \tag{10}$$

where $\tilde{E}_{zs}$ and $\tilde{\gamma}_f$ are the adjoint variables of E_{zs} and γ_f, respectively; $\tilde{\tilde{E}}_{zs}$ and $\tilde{\tilde{\gamma}}_f$ are the test functions of $\tilde{E}_{zs}$ and $\tilde{\gamma}_f$, respectively; $\mathcal{H}(\Omega)$ and $\mathcal{H}(\Omega_d)$ are the first-order Hilbert functional spaces defined on Ω and Ω_d, respectively; $Re(\cdot)$ and $Im(\cdot)$ are the operators used to extract the real part and imaginary part of a complex function, respectively. And $\delta\Psi_{Er}$ in Eq. 8 is the first-order variational of Ψ_{Er}

$$\delta\Psi_{Es} = -\int_{\Omega_d}\tilde{\gamma}_f\delta\gamma\,\mathrm{d}\Omega \tag{11}$$

with $\tilde{\gamma}_f$ derived by solving the adjoint equations

$$\begin{aligned}
&\int_\Omega \frac{2\left(E_{zs}+E_{zi}\right)^*}{\Psi_{Er0}}\tilde{\tilde{E}}_{zs} - \mu_r^{-1}\nabla\tilde{E}_{zs}^*\cdot\nabla\tilde{\tilde{E}}_{zs}\\
&+k_0\epsilon_r\tilde{E}_{zs}^*\tilde{\tilde{E}}_{zs}\,\mathrm{d}\Omega - \int_{\partial\Omega} jk_0\sqrt{\epsilon_r\mu_r^{-1}}\tilde{E}_{zs}^*\tilde{\tilde{E}}_{zs}\,\mathrm{d}\Gamma = 0,\\
&\int_{\Omega_d} r^2\nabla\tilde{\gamma}_f\cdot\nabla\tilde{\tilde{\gamma}}_f + \tilde{\gamma}_f\tilde{\tilde{\gamma}}_f + k_0\frac{\partial\epsilon_r}{\partial\gamma_p}\frac{\partial\gamma_p}{\partial\gamma_f}\Big[Re\left(E_{zs}+E_{zi}\right)\\
&Re\left(\tilde{E}_{zs}^*\right) - Im\left(E_{zs}+E_{zi}\right)Im\left(\tilde{E}_{zs}^*\right)\Big]\tilde{\tilde{\gamma}}_f\,\mathrm{d}\Omega = 0,\\
&\forall\tilde{\tilde{E}}_{zs}\in\mathcal{H}(\Omega),\ \forall\tilde{\tilde{\gamma}}_f\in\mathcal{H}(\Omega_d)
\end{aligned} \tag{12}$$

On numerical implementation of the solving procedure, the equations are discretized by the finite element method, which is implemented in the commercial package (COMSOL Multiphysics) [27].

Results and Discussion

To demonstrate the robustness of the inverse design method, the resonator cloaking performance is investigated, and the

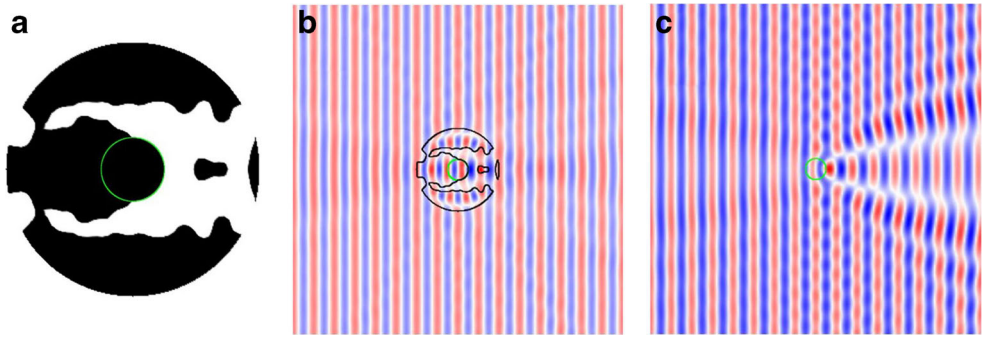

Fig. 2 Inversely designed resonator cloak for the uniform plane incident TE wave. The domain enclosed with the green circular line is the resonator. **a** is the inversely designed resonator cloak. **b** is the total field corresponding to the cloaked resonator. **c** is the total field corresponding to the uncloaked resonator. The corresponding optimized quotient is $q_E = 6.11 \times 10^{-2}$, where the scattering field is weakened to be 0.08-fold of that of the uncloaked case and the total field inside the resonator is strengthened 1.30-fold

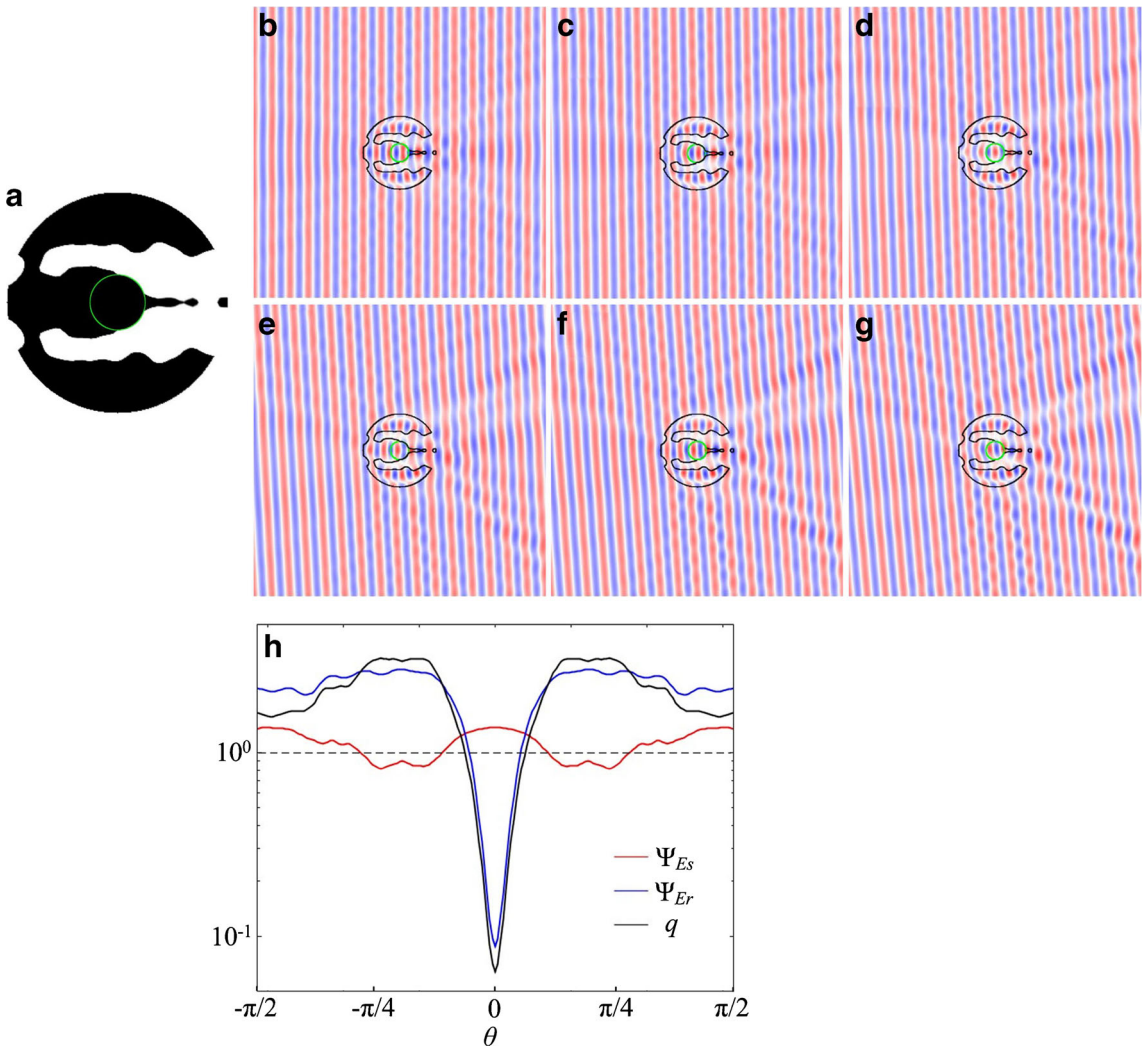

Fig. 3 Inversely designed resonator cloak for the uniform plane incident TE wave with incident angle bandwidth $-5° \sim 5°$. The domain enclosed with the green circular line is the resonator. **a** is the inversely designed resonator cloak. **b**-g is the total field corresponding to the uncloaked resonator with incident angle 0°, 1°, 2°, 3°, 4° and 5°, respectively. **h** the incident angle spectra of the designed resonator cloak

incident angle sensitivity is also considered. The method is applied further in the cases with dielectric materials SU8, Si and SiO_2 to reveal the origin of inversely designed resonator cloaking.

Inversely Designed Resonator Cloaking Performance

The dielectric material with relative permittivity $\epsilon_r = 2$ is chosen for both the resonator and cloak. The incident wavelength is set to be 0.6 m. The radius of the resonator and exterior radius of the ring-shaped design domain are set to be 0.5- and twofold of the incident wavelength, respectively. Then, the resonator cloak is derived as shown in Fig. 2, where the inversely designed resonator is shown in Fig. 2a, and the total fields for the cloaked and uncloaked resonator are plotted respectively in Fig. 2b and c. With the inversely designed resonator cloak shown in Fig. 2a, the scattering induced by the resonator is reduced to be 0.08-fold compared with that of the uncloaked case; and the filed is kept to resonate in the central domain with 1.30-fold enhancement. From the total field in Fig. 2b, one can conclude that the inversely designed resonator cloak achieves the phase matching by effectively weakening the scattering field in the outside surrounding and the total field is enhanced in the resonator by guiding and focusing the field in the cloak.

The resonator cloak in Fig. 2a is inversely designed for incident wave with fixed incident angle. Its performance has a strong dependence on the incident angle. Therefore, the incident angle-insensitive inverse design is implemented to extend the incident angle bandwidth. The inverse design procedure is implemented by setting the design objective to be the sum of equally weighted quotients corresponding to different incident angles valued in a specified incident bandwidth. By specifying the incident bandwidth to be $-5^\circ \sim 5^\circ$, the incident angle-insensitive inverse design of resonator cloak is derived as shown in Fig. 3a with total field distribution corresponding to different incident angles respectively shown in Fig. 3b-g. In Fig. 3h, the incident angle spectra of the inversely designed resonator cloak is plotted. These results demonstrate that reasonably good cloaking effect is achieved within the moderate angle range.

Application in the Cases with Dielectric Materials SU8, SiO_2 and Si

For photonic devices, SU8, SiO_2 and Si are widely used dielectrics with moderate and high relative permittivity. We chose the resonator and cloak materials from vacuum, SU8, SiO_2 and Si, and the corresponding resonator cloaks are derived as shown in Fig. 4, where the wavelength of the incident wave is 600nm with unity amplitude. On the optical properties of SU8, SiO_2 and Si, one can refer to the literatures [28–30]. The radius of the resonator and exterior

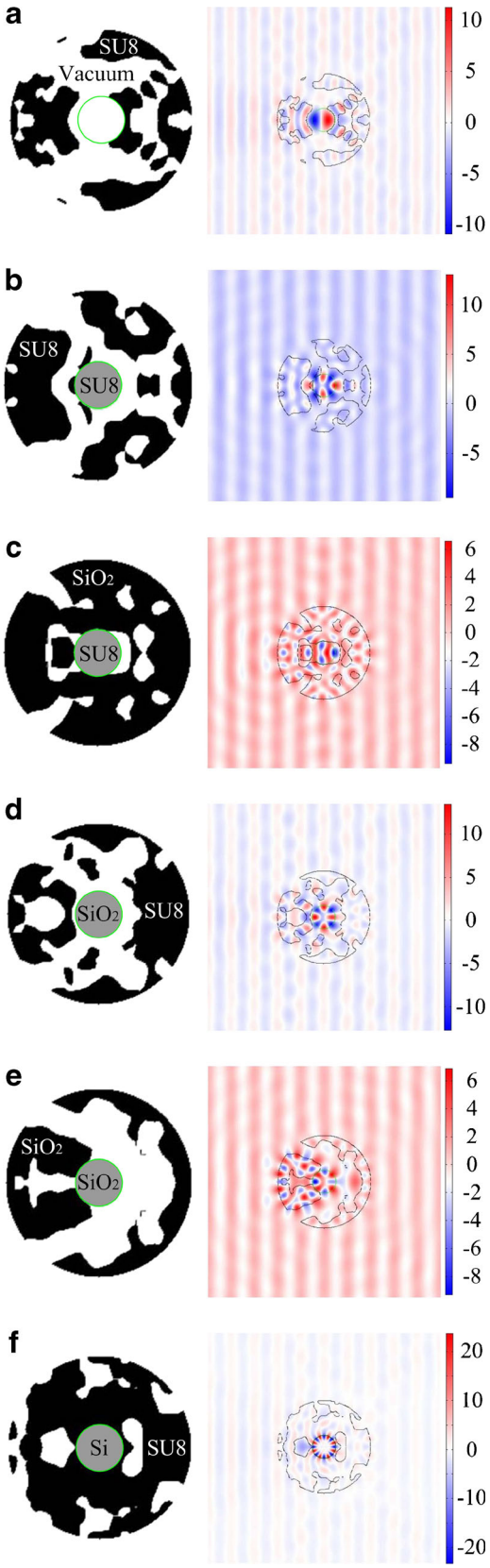

Fig. 4 Inversely designed resonator cloaking and the corresponding total field distribution, with resonator and cloak materials chosen from vacuum, SU8, SiO_2 and Si

radius of the ring-shaped design domain are set to be 0.5- and 2-fold of the incident wavelength, respectively. In the designed resonator cloaking, the cloaks simultaneously have the performance of guiding waves and matching the phase of the waves in the surrounding. For the case with resonator set to be vacuum, the wavelength in vacuum is relatively large, and the volume of the resonator domain is relatively small, then the Fabry-Pérot resonance, usually presented in resonator with low permittivity, is achieved by the cloak guiding, focusing and reflecting the incident wave (Fig. 4a). As the resonator is set to be Si, the wavelength of wave in Si with high permittivity is small enough and the Mie resonance, usually presented in resonator with high permittivity, is presented in the resonator (Fig. 4f). When the resonator is chosen to be SU8 or SiO_2 which has the moderate values of permittivity, the transmitting resonating modes can be regarded to be the hybrid of Fabry-Pérot resonance and Mie resonance.

On the fabrication of the structures with two dimensional layouts corresponding to the derived structural topology, several feasible nanofabrication processes are available for the future experimental tests. The feasible nanofabrication processes can include creating the patterns using the electron-beam lithography followed by dry etching, and depositing relevant dielectric materials using atomic layer deposition. And these nanofabrication processes have been reviewed in [31].

Conclusions

In conclusion, we have investigated the resonator cloaking using the topology optimization-based inverse design methodology. By setting the quotient between the outside surrounding scattering field energy and the total field energy in the central resonator, the cloak is inversely designed with various dielectric materials, and the motivation on enhancing or keeping the field inside the resonator and suppressing the induced scattering is achieved. With the dielectric cloak, the field energy is amplified in the resonator, the scattering field is weakened effectively in the surrounding vacuum, and the wave-guiding and phase-matching performance of the designed cloak achieves the resonator cloaking. The resonator cloaking inversely implemented using different dielectrics demonstrates that the resonator cloaking has the three types of performance, i.e. the Fabry-Pérot resonance cloaking, Mie resonance cloaking and hybrid resonance cloaking. We anticipate that our method can be used for designing other transformation optical devices, such as beam splitters, waveguide bends, and focusing lenses, in the future.

Acknowledgments This work is supported by the National Natural Science Foundation of China (No. 51405465, 51275504), the National High Technology Program of China (No. 2015AA042604), the Science and Technology Development Plan of Jilin Province and Changchun City (No. 20140201011GX, 20140519007JH, 15SS12). The authors are grateful to Professor K. Svanberg for the supply of the MMA codes. The authors are also grateful to the reviewers' kind attention and valuable suggestions.

References

1. Alu A, Engheta N (2009) Cloaking a sensor. Phys Rev Lett 102:233901
2. Alu A, Engheta N (2010) Cloaking a receiving antenna or a sensor with plasmonic metamaterials. Metamaterials 4:153–159
3. Pendry JB, Schurig D, Smith DR (2006) Controlling electromagnetic fields. Science 312:1780–1782
4. Leonhardt U (2006) Optical conformal mapping. Science 312:1777–1780
5. Gallina I, Castaldi G, Galdi V, Alu A, Engheta N (2010) A Transformation-optics-inspired route to sensor invisibility based on cloak/anti-Cloak interactions. URSI International Symposium on Electromagnetic Theory:668–671
6. Chen H, Chan CT, Sheng P (2010) Transformation optics and metamaterials. Nat Mater 9:387–396
7. Ni X, Wong Z, Mrejen M, Wang Y, Zhang X (2015) An ultrathin invisibility skin cloak for visible light. Science 349:1310–1314
8. Guo Y, Yan L, Pan W, Shao L (2016) Scattering engineering in continuously shaped metasurface: An approach for electromagnetic illusion. Sci Rep 6:30154
9. Pu M, Zhao Z, Wang Y, Li X, Ma X, Hu C, Wang C, Huang C, Luo X (2015) Spatially and spectrally engineered spin-orbit interaction for achromatic virtual shaping. Sci Rep 5:9822
10. Bendsoe MP, Sigmund O (2003) Topology optimization-theory, methods and applications. Springer, Berlin
11. Borrvall T, Petersson J (2003) Topology optimization of fluid in Stokes flow. Int J Numer Meth Fluids 41:77–107
12. Nomura T, Sato K, Taguchi K, Kashiwa T, Nishiwaki S (2007) Structural topology optimization for the design of broadband dielectric resonator antennas using the finite difference time domain technique. Int J Numer Meth Engng 71:1261–1296
13. Duhring MB, Jensen JS, Sigmund O (2008) Acoustic design by topology optimization. J Sound Vibration 317:557–575
14. Gersborg-Hansen A, Bendsoe MP, Sigmund O (2006) Topology optimization of heat conduction problems using the finite volume method, Struct. Multidisc Optim 31:251–259
15. Otomori M, Yamada T, Izui K, Nishiwaki S, Andkjær J (2012) A topology optimization method based on the level set method for the design of negative permeability dielectric metamaterials. Comput Methods Appl Mech Engrg 237-240:192–211
16. Sigmund O (1996) Materials with prescribed constitutive parameters: an inverse homogenization problem. Int J Solids and Struct 31:2313–2329
17. Deng Y, Liu Z, Zhang P, Liu Y, Wu Y (2011) Topology optimization of unsteady incompressible Navier-Stokes flows. J Comput Phys 230:6688–6708
18. Andkjær J, Sigmund O (2011) Topology optimized low-contrast all-dielectric optical cloak. Appl Phys Lett 98:021112
19. Sigmund O, Hougaard KG (2008) Geometric properties of optimal photonic crystals. Phys Rev Lett 100:153904

20. Zhou S, Li W, Sun G, Li Q (2010) A level-set procedure for the design of electromagnetic metamaterials. Opt Express 18:6693–6702
21. Deng Y, Liu Z, Song C, Hao P, Wu Y, Liu Y, Korvink JG (2016) Topology optimization of metal nanostructures for localized surface plasmon resonances. Struct Multidiscip Optim 53:967–972
22. Deng Y, Liu Z, Song C, Wu J, Liu Y, Wu Y (2015) Topology optimization based computational design methodology for surface plasmon polaritons. Plasmonics 10:569–583
23. Lazarov B, Sigmund O (2011) Filters in topology optimization based on Helmholtz type differential equations. Int J Numer Methods Eng 86:765–781
24. Guest J, Prevost J, Belytschko T (2004) Achieving minimum length scale in topology optimization using nodal design variables and projection functions. Int J Numer Methods Eng 61:238–254
25. Sigmund O (2007) Morphology-based black and white filters for topology optimization. Struct Multidiscip Optim 33:401–424
26. Deng Y, Korvink JG (2016) Topology optimization method for three dimensional electromagnetic waves. Proceedings of Royal Society A 472:20150835
27. http://www.comsol.com
28. Aspnes DE, Studna AA (1983) Dielectric functions and optical parameters of Si, Ge, GaP, GaAs, GaSb, InP, InAs, and InSb from 1.5 to 6.0 eV. Pys Rev B 27:985–1009
29. http://refractiveindex.info
30. http://www.filmetrics.com
31. Boltasseva A, Shalaev VM (2008) Fabrication of optical negative-index metamaterials: recent advances and outlook. Metamaterials 2:1–17